

A specification of a flywheel battery for a rural South African village

Richard Okou

Department of Electrical Engineering, University of Cape Town

Adoniya Ben Sebitosi

Department of Mechanical and Mechatronics Engineering, University of Stellenbosch, South Africa

Pragasen Pillay

Department of Electrical and Computer Engineering, Concordia University, Canada

Abstract

The strong growth rates in the installed capacities of renewable energy technologies that have been posted in recent years demonstrate their capacity in the mitigation of green house gas emissions and climate change. The majority of these growths, however, have been realised in grid connected first world programs and do not require provision for energy storage. Most African rural areas are still far from the grid. Many upcoming developments such as cellular network repeater stations and health clinics must be operated from independent off grid PV installations. The intermittence of the resources dictates that reliable energy storage must be provided. The lead acid battery is currently the only available option but has well documented maintenance and disposal problems. The flywheel battery is an old technology that is re-emerging with a strong promise and could address the shortcomings of the lead acid battery. In this paper, a case study of a rural South African village load is depicted. Using a real utility database a possible specification for an electro-mechanical battery is derived. The authors further highlight the areas that will need future developments.

Keywords: *energy storage, flywheel system, rural energy, South Africa*

1. Introduction

Most rural electric loads are characterized by poor load factors with virtually no coincidence between generation and consumption. In the case of PV, for example, power generation is by daytime, while the lighting and infotainment dominated loads are almost entirely by night. Cynics have aptly likened operating such a system, without adequate storage, to milking a cow without a bucket. Energy storage remains by far the biggest challenge in rural electrification.

Electrical energy storage technology in sub-Saharan Africa is almost exclusively by chemical batteries, particularly the automotive lead acid type (Buchmann, 2001). The batteries have low initial prices but this is deceptive, as their short life spans imply routine replacement expenses. This increases the burden on the environment due to the frequent disposal of toxic materials. In addition, they have low depth of discharge capabilities and thus larger than necessary capacities are required, which further erodes their apparent cost advantage. There are certain battery types, which have labels like “solar batteries” with somewhat enhanced depths of discharge but this often comes with trade-offs.

Hunt (1998) refers to an inextricable link between power, energy and lifespan (in both age and charge-discharge cycles) that continues to baffle chemical battery researchers. Whenever any one of these three functions is enhanced, at least one of the remaining two deteriorates. For example, in order to deliver a required peak transient power, the design must offer high electrolyte to plate exposure but this in turn increases self-discharge rates and, hence, reduces the available energy. Ambient temperatures also affect charging characteristics and

general performance. Other issues range from simple ones like water loss (or drying up) to more abstract ones like electrolyte stratification. In renewable energy installations, batteries are often connected in series strings and charged while in use. Due to disparities in chemistry, different cells charge at different rates and the necessary equalization to allow the slow charging sections to top up cannot be carried out feasibly. Moreover due to the stochastic nature of resources, many generators are fitted with maximum power point trackers which often conflict with the set 'optimum' battery charging rates and results in dumping of excess power even when batteries are not fully charged. In addition, if battery cells should be kept at overcharge (say above 2.45volts in case of lead acid) for long periods, grid corrosion results. On the other hand, in cases of sustained low insolation and high load demand, the batteries will have to be exposed to long periods of deep discharge. This could lead to (the aforementioned) sulfation: a state that renders recharging difficult and at times impossible (Buchmann, 2001). Moreover, all chemical batteries suffer from high discharge shock, which compromises their life spans. Consequently, chemical batteries require expensive and highly skilled maintenance in order to yield maximum life. Skilled manpower and disposable income are rare commodities in African rural areas.

The flywheel (Hebner and Aanstoos, 2000; Post, 1996, Post *et al.*, 1993; Patel, 1999, Nasa, Bitterly 1998; Herbst *et al.*, 1998; Hayes *et al.*, 1999) is an age-old technology that has seen recent revival and could subsequently evolve to address the above concerns. The use of flywheels as reaction wheels (like porter's wheels) dates back to biblical times. The first electromechanical battery was however, only reported in the late 1940's in the urban Swiss vehicle called the gyro bus. Even then further research did not pick up until the 1970's, mainly for outer space programs but still kept a relatively low profile. The early 1990's saw a new revival as international political pressure increased demand for environmentally benign technologies. This was augmented by developments in strong lightweight materials, magnetic technology and solid-state electronics (Tsung *et al.*, 1993; Arnold *et al.*, 2001; Baaklini *et al.*, 2000; Tsai and Wu, 1971; Seireg *et al.*, 1970; Sung *et al.*, 1998; Halbach, 1980; Ofori and Lang, 1995). Subsequently, flywheel battery technology was shortlisted as one of the candidate technologies by the Partnership for a New Generation of Vehicles (PNGV) in the mid 1990's (Nap 1999, Sebitosi and Pillay 2003).

Potential attributes of the technology include long life spans, ability to charge or discharge at very high power rates through very deep cycles, no deterioration in performance with number of charge/recharge cycles and freedom from most of the chem-

ical battery encumbrances. This technology has the potential to challenge the energy density of petroleum.

This paper will examine the possibility of using the environmentally benign electromechanical flywheel battery in rural sub-Saharan Africa. Conclusions will then be drawn as to the possibility of adopting the flywheel battery as electrical energy storage for rural requirements.

2. Kinetic energy storage

In principle, a flywheel stores energy in kinetic form, in a rotating wheel that is suspended on frictionless bearings in an aerodynamically drag-free vacuum enclosure.

The kinetic energy stored in a moving body is proportional to its mass and the square of its linear velocity.

$$KE = \frac{1}{2}mv^2 \quad (1)$$

When transformed into rotational motion one must consider the moment of inertia J . For the solid cylinder (Figure 1) rotating about its axis, the moment of inertia is defined as $J = \sum m_i r_i^2$, the sum of all elemental masses multiplied by the square of their distances from the rotational axis. As the sizes of these particles tend to zero they are virtually cubic with dimensions $\delta\omega$, δr and h .

$$J = \int_{\theta=0}^{2\pi} \int_{r=0}^R \rho h \cdot d\omega \cdot dr \cdot r^2 \quad (2)$$

For a solid cylinder:

$$J = \frac{1}{2}mr^2 \quad (3)$$

And that for a hollow cylindrical system, as is typical of flywheels:

$$J = \frac{1}{2}m(r_o^2 + r_i^2) \quad (4)$$

Where r_i and r_o are the inner and outer radii respectively and the kinetic energy stored KE is given in equation (5).

$$KE = \frac{1}{2}J\omega^2 = \frac{1}{4}m(r_o^2 + r_i^2)\omega^2 \quad (5)$$

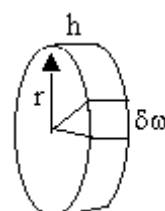


Figure 1: A solid cylinder with radius r and height h

The energy grows in proportion to the flywheel mass and the square of the angular velocity. So there is more emphasis on angular velocity rather than mass.

Consider a special case of a thin rotating ring. Its moment of inertia, J is given by equation (4). But as the thickness tends to zero $r_i = r_o = r$ and

$$J = \frac{1}{2}m(r_i^2 + r_o^2) = mr^2$$

But $v = r\omega$

So kinetic energy:

$$KE = \frac{1}{2}mv^2 = \frac{1}{2}mr^2\omega^2 = \frac{1}{2}J\omega^2 \quad (6)$$

Where v is the linear velocity of a particle, r is the mean radius of the ring; m is its mass and ω its angular velocity.

The spinning subjects the rotor to stresses in proportion to the square of the angular velocity. These stresses can lead to failure. So, the maximum speed and therefore the maximum amount of energy storage attainable by the rotor is governed by its tensile strength.

$$KE = \frac{1}{2}m\frac{\sigma_h}{\rho} = \frac{1}{2}J\omega^2 \quad (7)$$

Where σ_h is the maximum allowable hoop stress for the ring, ρ is the density of the material.

The above expressions are only true for a thin ring. To get the total kinetic energy of a composite disk one would, in theory, have to sum up the energy in the nearly infinite thin rings. In practice the factors that determine rotor failure are much more complex. There is still lack of adequate experience and test data and much is still the subject of intense research. For example, while different composite flywheel designs may exhibit clearly different types of failure, similar designs may not necessarily fail in a similar manner.

3. The motor generator

In order to transfer energy to and from the spinning disk, a motor generator is used. The most popular choice is a permanent magnet synchronous machine, with an outer rotor design largely due to its high efficiency. The heart of this machine is an ironless magnetic array: an innovation by Klaus Halbach (Halbach, 1980) which reduces the stator losses to just the copper losses. The outer rotor is integrated into the flywheel, forming one unit instead of a machine with an attached flywheel.

An ideal Halbach cylinder is defined as an infinitely long structure where the magnitude of the magnetisation is constant and its orientation turns continuously. At an angular position ϕ in the cylinder, measured clockwise from the y -axis, the magnetisation has an orientation 2ϕ . The collective

result is a uniform magnetic field, B^y in the y direction within the cylinder bore and a zero field outside the cylinder. The field is dependent only on the ratio between the inner r_i and outer r_o radii of the cylinder (or the difference between their natural logarithms) as given by equation (8).

$$B_y = J_r \ln\left(\frac{r_o}{r_i}\right) = J_r (\ln r_o - \ln r_i) \quad (8)$$

where J_r is the remnant field of the magnetic material of the cylinder.

In practice, however, approximations of this ideal design are constructed from a finite number, N , of short segments of high quality (rare-earth) magnets and systematically rotated to form an array as shown in Figure 2. It has the advantage of cutting down on cost of magnetic material as well as improving their stress performance. They can be arranged depending on the number of poles required. These magnets form the inner part of the motor rotor as illustrated in Figure 3. Unlike the ideal case, however, there's a finite stray field on the outside. There is also a possibility of some mild eddy current in the array magnets due to the current in the stator winding. In the illustrated practical dipole (Figure 2) the magnetic field B (in the bore) is dependent on the number of magnet elements used, as well. It is given by Halbach's theoretical treatment as equation (9).

$$B = J_r \ln\left(\frac{r_o}{r_i}\right) \eta \quad (9)$$

Where

$$\eta = \left[\frac{\sin(2\pi/N)}{(2\pi/N)} \right]$$

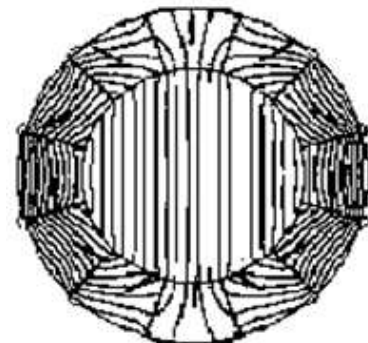


Figure 2: Magnetic field distribution of a dipole Halbach array

As illustrated in Figure 3, the winding is on the inner core which forms the stator, while the magnet array is moulded with the composite rotor with which it spins. The losses to be expected from the configuration in Figure 3 are copper losses in the

stator windings, rotor bearing losses and no air drag losses in the vacuum chamber. Therefore, the deceleration torque on no load (which is the self-discharge factor for the battery) is constant and not dependent on rotor speed. Bearing losses are minimized by the use of magnetic rather than mechanical bearings. The copper winding for the armature is sometimes made from tubing to enable the circulation of cooling oil.

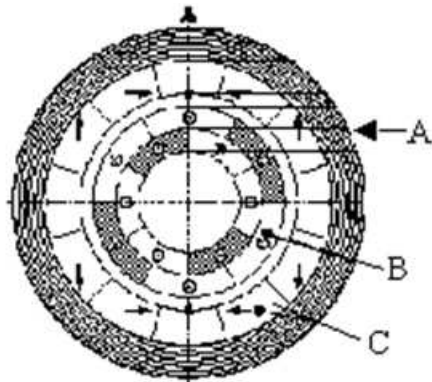


Figure 3: A cross-section of an ironless motor generator (complete) with the composite rotor (A is the composite ring, B is the electrical winding 3-phase 4 pole, C is the magnet array)

The performance of the machine can then be summarized as follows. Since the field strength, B and the depth of the magnetic ring, l are constant, the torque developed during charging will depend on charging (armature) current.

So for the dipole above, with I_{eff} as the effective current and l, as the magnetic depth, the torque T is given by

$$T = B \frac{\sqrt{2}}{3} q l I_{eff} \sin\left(\frac{\pi}{q}\right) \quad (10)$$

Where, q is the number of phases for the machine.

The choice of a dipole version of the Halbach's magnet arrangement has been further supported in Post (1993) on the grounds that it makes the inductive coupling between the magnets and the windings relatively insensitive to the radial gap between them. This eases the mechanical clearance between them.

Ofori-Tenkorang *et al.* (1995) showed that the torque developed by a permanent magnet synchronous motor using the Halbach array (with an ironless core) is much higher than for a conventional array using the same weight and type of magnets.

4. Power electronics

The function of this sub-system is to condition the power to and from the generator (Amc, Bowler). This is necessitated by the fact that the flywheel motor generator has a continually variable voltage and frequency. Likewise, the levels of power from

an external source like a wind turbine or a PV generator often vary with time. Currently the most popular drive components are insulated gate bipolar transistors (IGBT). These are driven by appropriate control electronics. Figure 4 illustrates a typical 3-phase flywheel battery /power conditioner scenario.

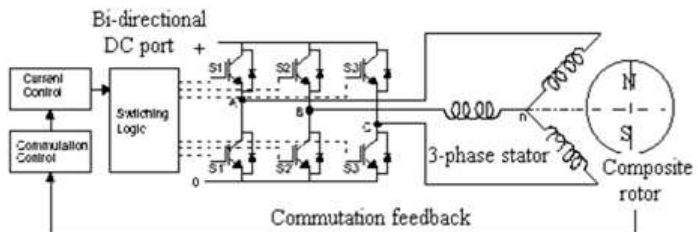


Figure 4: Flywheel motor/generator connected to a DC bus via a power-conditioning configuration using a 6-digit pulse topology

The DC port is bi-directional depending on whether the battery is in generating or charging mode and could be connected directly to a DC generator and DC load or via an inverter to an AC load. In Figure 4 the IGBTs are designated as S1, S2, etc. They are operated by micro-controllers in a 6-pulse bridge topology. Commutation is enabled by rotor position feedback obtained from Hall Effect sensors built into the stator to detect the position of the rotor magnetic field.

The mounting is such that they each generate a square wave with 120° phase difference over one electrical cycle of the motor (Figure 5). The amplifier drives two of the three motor phases with DC current during each specific Hall sensor state. The technique is reputed to result in a very cost-effective amplifier (Amc).

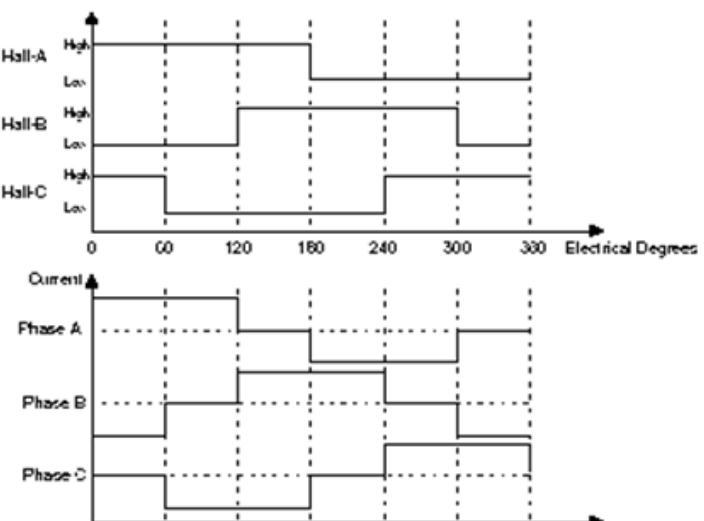


Figure 5: Hall sensor based commutation

5. Possible flywheel battery specification for rural application

From what has been mentioned, the energy stored in a flywheel battery is proportional to the system

moment of inertia, J and the square of the rotor system angular speed (for convenience, details of the power conditioning equipment will assume to be ideal). If the rated angular speed of the flywheel rotor is ω_R , then maximum energy that can be stored is E_F such that

$$E_F = \frac{1}{2}J\omega_R^2 \quad (11)$$

If the maximum permissible depth of discharge for the battery is 90%, then there would be a balance of 10% of the energy at which point the rotor speed would be ω_o , such that

$$\omega_o = \sqrt{\frac{\omega_R^2}{10}} = 0.316\omega_R \quad (12)$$

The terminal voltage of the flywheel generator is linearly proportional to the rotor speed. Therefore, the terminal voltage at 90% depth of discharge (DOD) would be 31.6% of the full speed voltage, V_R , which is the rated voltage. Considering the internal impedance to be negligible, the open circuit voltage should be approximately equal to the output bus voltage even at full load. Let the flywheel battery be designed to deliver its continuous rated power P_R over the entire operating speed range. Then by Ohm's law, the current drawn at the minimum operating speed would be the highest permissible or rated current.

Figure 6 is a 24-hour electric load profile of a rural household from a database of the South African National Rationalised Specifications (NRS) Load Research Project for Garagapola village. It will be assumed that this represents a typical daily load profile. The daily peak load is 7.85A, with an average of 0.66A and hence, a load factor of 8.4%. The total energy consumed by the household at a supply voltage of 230V was $(24 \times 0.66 \times 230) = 3643.2$ Wh.

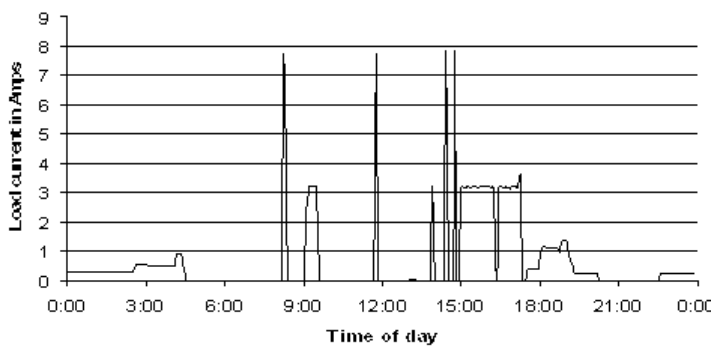


Figure 6: A 24-hour load profile recorded by NRS for a household in Garagapola village

Consider the above to be an off-grid rural household operating from a stochastically distributed renewable energy source, which would require a storage battery. It is regular practice for off-grid

storage facilities to be specified for several autonomous days each being equivalent to the average daily requirement. So if this household were to have a storage capacity to last for 2 autonomous days (plus one normal day) then the available battery capacity would be $(3643.2 \times 3) = 10929.6$ Wh. Since the maximum allowable depth of discharge for the flywheel battery is 90%, then the flywheel battery capacity must be $(10929.6 \text{ Wh} \div 90\%) = 12144$ Wh. This capacity, however, does not take losses into account. If a battery charge-discharge efficiency of 80% is assumed (Post, 1996) then final value is $(12144 \text{ Wh} \div 0.8 = 15180 \text{ Wh})$.

Let the flywheel be designed for a rated speed ω_R of 60 000 revolutions per minute, which is 2000π radians per second.

From the above, $15180 \text{ Wh} = 3600 \times 15.18 \text{ kilo joules} = \frac{1}{2}J(2000\pi)^2$ (where, J is the flywheel rotor system inertia).

Therefore,

$$J = 2.77 \times 10^{-3} \text{ kg} - \text{m}^2$$

Household peak power demand = $(7.85 \times 230) = 1.81 \text{ kW}$. Allowing for a margin of error, the battery could be rated for continuous power of 2 kW. As stated, the validity of this specification is required for the entire operating speed range and must therefore be applicable at the minimum state of charge. In this case, when there is only 10% of storage capacity and at a rotor speed (and hence at a bus voltage) of 31.6% of the rated.

Let the full rated voltage be 100V, then at 10% state of charge (SOC) the voltage will be 31.6V.

Then the rated current, I_R must equal to the rated power divided by the minimum operating voltage

$$I_R = 2000/31.6 = 63.30 \text{ Amp}$$

The load torque exerted on the flywheel is proportional to the generator current (which is the load current) and therefore the maximum load torque will be at the rated load current. This should be true for both charging and discharging modes. But power, P is the product of torque, T and angular speed, ω .

Therefore,

$$P = T\omega = K_F q I_{eff} \omega \quad (13)$$

Where,

$$K_F = B \frac{\sqrt{2}}{3} l \sin\left(\frac{\pi}{q}\right)$$

is the torque constant and qI_{eff} = total load current.

From equation (12) the minimum flywheel speed is given by ω_o such that

$$\omega_o = 0.316\omega_R = 0.316\left(\frac{2\pi \cdot 60000}{60}\right) = 632\pi$$

Radians per second.

Then from equation (13) the machine torque constant, K_F can be calculated using rated power at minimum speed.

$$K_F = \frac{P}{632\pi \cdot qI_{eff}} = \frac{2000}{632\pi \cdot 63.3} = 0.02 \quad (14)$$

Let the design be a three-phase ($q=3$) machine

$$K_F = B \frac{\sqrt{2}}{3} (3 \cdot l \cdot \sin \frac{\pi}{3}) = B \sqrt{\frac{2}{3}} \cdot l = 0.02 \quad (15)$$

From equation (9)

$$B = J_r \ln \left(\frac{r_o}{r_i} \right) \left(\frac{\sin \left(\frac{2\pi}{N} \right)}{\left(\frac{2\pi}{N} \right)} \right)$$

Using the dipole in Figures 2 and 3, the number of magnets used is 12. Let $N = 12$. The remanent field of grade 32 rare earth, Nd-Fe-B (Neodymium Iron Boron) is typically $J_r = 1.15$ tesla.

$$B = 1.15 \ln \frac{r_o}{r_i} \left(\frac{\sin \frac{\pi}{6}}{\frac{\pi}{6}} \right) = \frac{3}{\pi} \ln \frac{r_o}{r_i}$$

In Post (1996) the value for $\frac{r_o}{r_i}$ is assumed to be 1.5. Using this figure the value of the dipole strength, B is

$$B = \frac{3}{\pi} \times \ln 1.5 = 0.39 \text{ tesla}$$

From equation (13), the expression for the axial length l , can be found

$$l = \frac{0.02}{B \sqrt{\frac{2}{3}}} = 0.05 \text{ meters}$$

Since the rated power of 2000W must be available at minimum angular speed of 632π then the maximum torque T is given by:

$$T = \frac{2000}{632\pi} = 1.01 \text{ Nm}$$

Let the battery be required to maintain a maximum self-discharge rate of 90% per month on no-load. Then the total amount of energy lost this way must be $\leq 90\%$ of full storage capacity $\leq 90\% \times 15180 \text{ Wh} = 13662.9 \text{ Wh}$. Therefore, the average self-discharge rate = 13662.9 Wh in (24×30) hours or 18.98 W.

Assuming a total absence of air drag in the containment chamber, these losses are due to bearing friction and proportional to the rotor mass. The resulting deceleration torque T_d is therefore constant and is equal to the product of the average speed over the deceleration range and the average rate of loss of power. Speed range is 2000π to 632π radians per sec. So the average speed is 1316π rad/sec. $T_d \cdot 1316\pi = 18.98W$, therefore the permissible bearing frictional torque should not

$$\text{exceed } T_d = \frac{18.98}{1316\pi} = 4.6 \times 10^{-3} \text{ Nm}$$

From equation (4),

$$J = \frac{1}{2} m (r_o^2 + r_i^2)$$

Let the inner radius $r_i = 25 \text{ mm}$. From Post (1993) it is assumed that:

$$\frac{r_o}{r_i} = 1.5$$

Using the same assumption the outer radius

$$r_o = 1.5 \times 25 = 37.5 \text{ mm}$$

Therefore, the rotor mass =

$$m = \frac{2J}{(r_o^2 + r_i^2)} = 2.73 \text{ kg}$$

6. Flywheel structure and magnetic bearings

A configuration structure of total flywheel system and rotor mass is proposed as shown in Figure 7. The total system and the hollow shaft are fixed in between two plates to ensure the stability of the flywheel system. The Halbach machine is embedded in the flywheel and the entire system levitated. The stator winding are fixed on the shaft.

There are numerous types and configurations of magnetic bearings. The choice of this combination was to suite the flywheel design, support the total weight of the rotor and accommodate a Halbach array PM machine. The magnet ring pairs at the bottom of system, as shown in Figure 7, are applied to levitate total weight of flywheel mass and other peripheral components. The stator of radial active magnetic bearing is appended by 6 suspension steel

rods to ensure the stability of the stator. The axial magnetic bearings are used to keep the system axially stable. The rotor of axial magnetic bearing is connected with the rotor of radial magnetic bearing by the axial bearing radial bearing coupling. All these three parts are levitated and rotate with the flywheel.

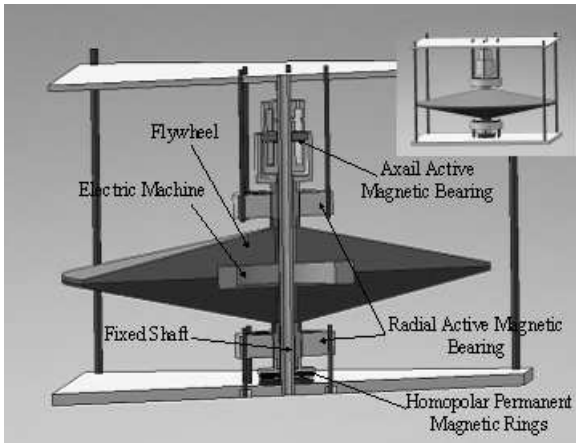


Figure 7: Flywheel structure

6.1 Repulsive magnetic force analysis of Homopolar PM magnets ring pairs

The repulsive force between two homopolar permanent magnetic ring pairs, as shown in Figure 8, are applied to suspend the weight of the flywheel and this reduces the losses in the coil and iron losses in the active magnetic bearing. In order to reduce the dimension and increase stiffness of magnetic bearing, this type of magnetic ring is designed from high remnant flux density and high coercive force material NdFeB.



Figure 8: Homopolar permanent magnetic suspension ring pair

The force between the two magnetic rings can be calculated by the magnetic charge method, equivalent current method, Maxwell equation method and virtual work method. In this design process, the equivalent current method is applied as shown in Figure 9.

A virtual magnet plate is assumed inside the ring to form a large magnet plate. Then, the repulsive magnetic force between the two large plates, between one virtual magnet plate and one large plate and between two virtual magnet plates can be calculated by the equivalent current method.

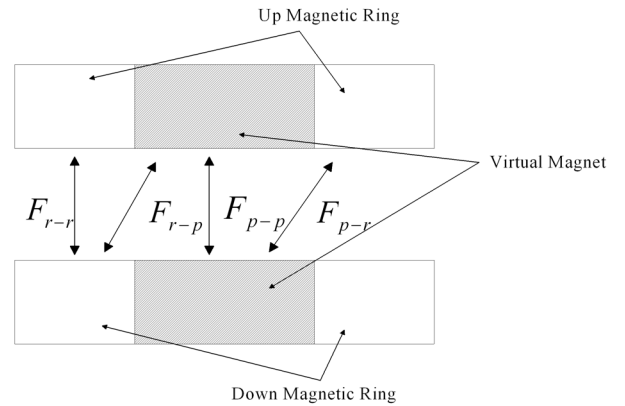


Figure 9: Virtual method to calculate magnetic force

A model with various lengths of the airgap was simulated in Finite Element (FE) software Flux 2D/3D and compared with the equivalent current method. The results are shown in Figure 10. From Figure 10, the repulsive magnetic force between the two magnet ring pairs calculated by the equivalent current method matches the FE method closely. Therefore, by applying the equivalent current method, the relationship between the weight of the flywheel and the length of airgap can be optimized.

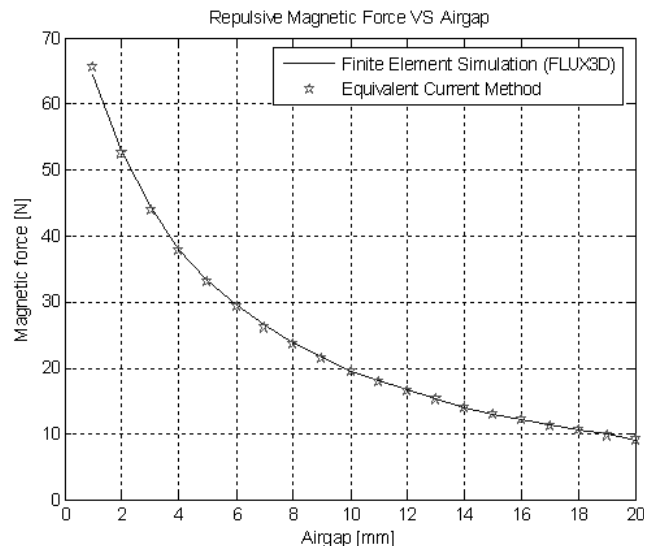


Figure 10: Repulsive magnetic force VS airgap

6.2 Attractive magnetic force analysis of axial active magnetic bearings

This section illustrates the design and performance of the axial active magnetic bearings. As shown in Figure 11, when a current is applied in the coil, the flux passes through the shell of the York and the plate to induce the magnetic attractive force as shown in Figure 12.

The equivalent magnetic circuit is shown in Figure 13. In order to simplify the model, only the

slot leakage and edge effect are taken into account. The magnetic saturation is neglected.

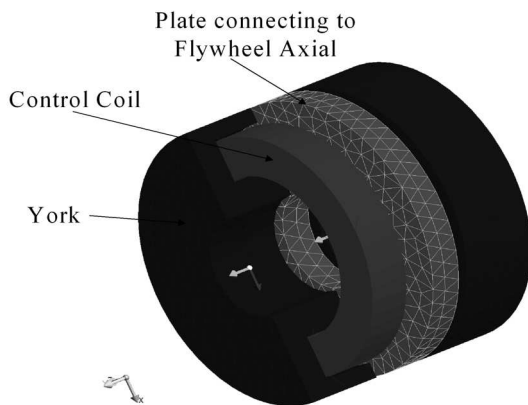


Figure 11: Active axial magnetic bearing

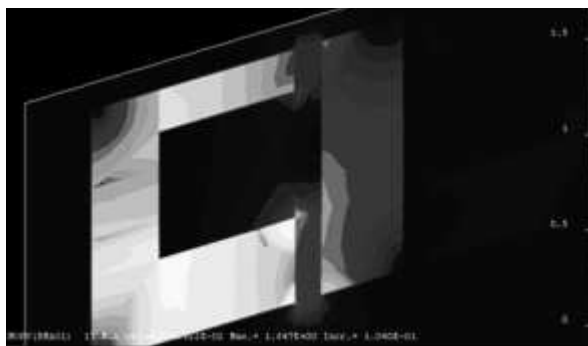


Figure 12: Flux in the magnetic bearing

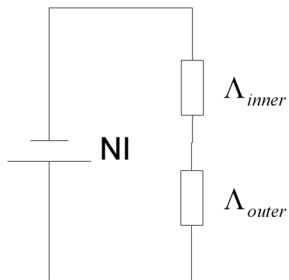


Figure 13: Equivalent magnetic equation of active axial magnetic bearing

The structure is analyzed and simulated in Flux2D/3D by FE method. The result is shown in Figure 14.

The results from the two methods are closely correlated. For a large excitation current, the simulation result is smaller than the analysis result, which is anticipated because of magnetic saturation in the magnetic material. Furthermore, this current Vs force curve can be applied in transient analysis of flywheel.

6.3 Attractive magnetic force analysis of radial active magnetic bearing

The structure and performance of the eight pole radial active magnetic bearing is simulated in

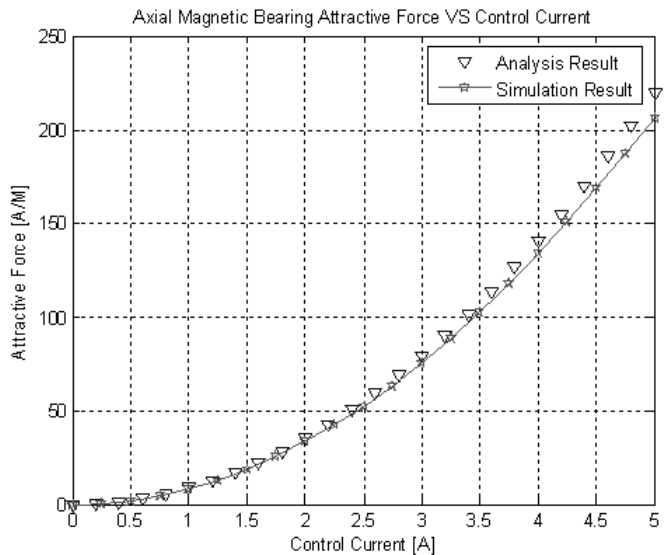


Figure 14: The attractive force of active axial magnetic bearing vs control current

Flux2D/3D. This is charged with control of the radial stability of the system. The structure of radial active magnetic bearing is shown in Figure 15. The inner part is the rotor and is coupled to the flywheel and shaft. The outer part is the stator of bearing and the middle is the coil.

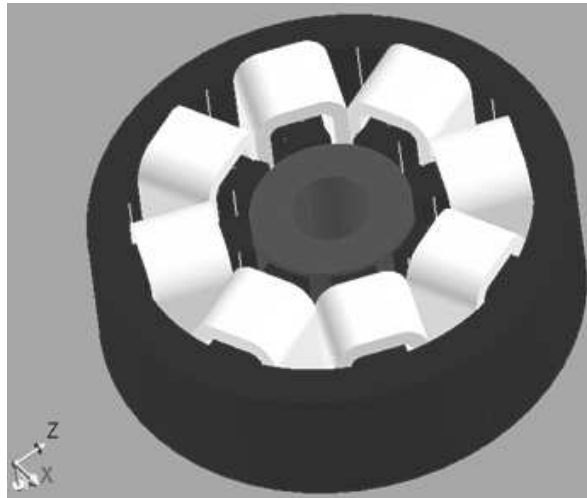


Figure 15: Eight pole radial active magnetic bearing

The 8 poles are separated into four sections to induce four direction attractive forces: Positive X, Negative X, Positive Y, and Negative Y. The coil in the two pole pairs are wound in contrary directions. This is done such that the flux passes from one pole into another one, rather than pass into other poles as shown in Figure 16.

In order to avoid the saturation in the steel, the flux density in the air gap is kept at 0.9T and this happens when the control current is 3.6A. The corresponding induced magnetic force is 200N as shown in Figure 17.

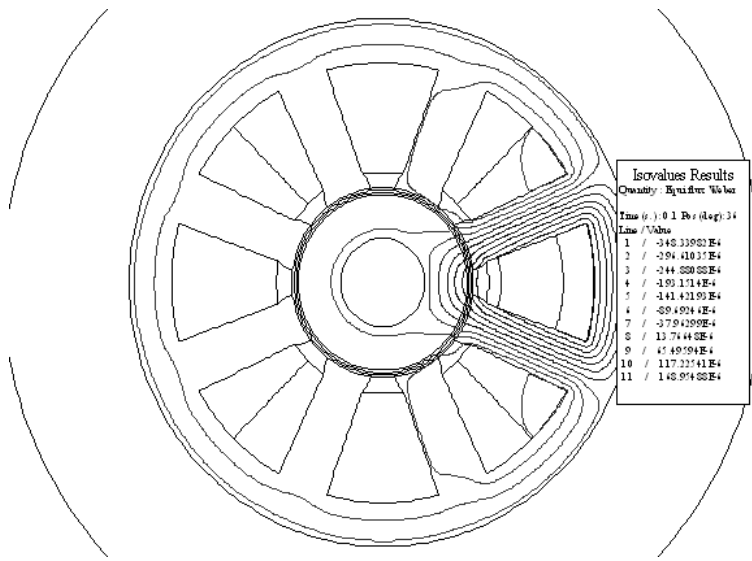


Figure 16: Flux in the radial magnetic bearing

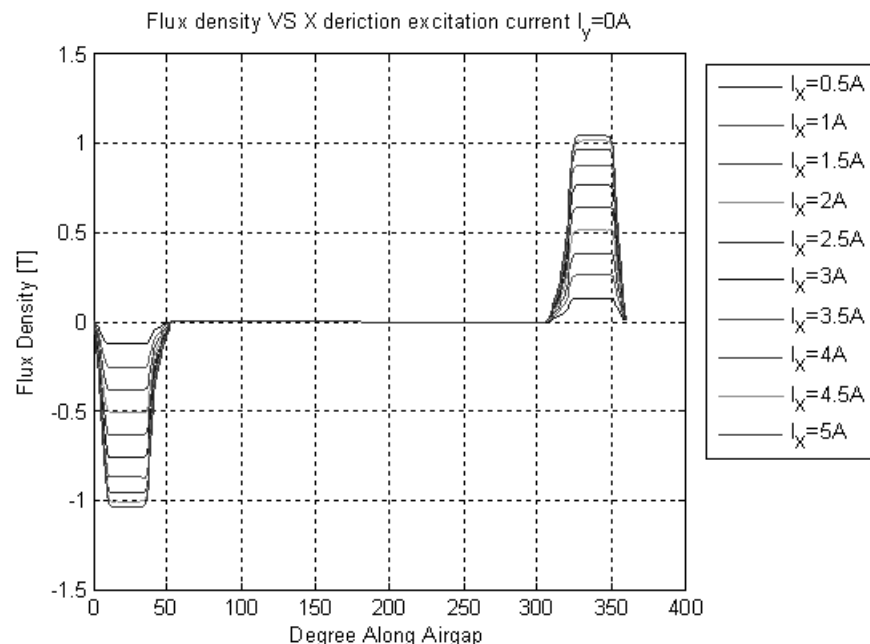


Figure 17: Flux density along the airgap versus X direction current

From Figures 16 and 17, almost all the flux passes through positive X direction pole pairs. In order to avoid the wrong flux circuit, the right pole of Positive Y direction poles pairs should be the same polarity as the upper pole of positive X direction pole pairs. The positive X, Y direction coil are excited by various control current. The various flux densities in the air gap are shown in Figure 17 and 18.

The analysis model of radial magnetic bearing was developed. The attractive force of X and Y direction is calculated and compared with Finite Element method with various control current as shown in Figures 19 and 20.

At the designed maximum current, the magnetic attractive force calculated by analysis method

matches the result of FE method perfectly as shown in Figure 19. When the control current is more than 3.6A the magnetic attractive force is more than 200N and the difference between two methods increases. This is reasonable, because in the analysis method, the magnetic intensity drop in the steel is neglected. At large working flux density, the steel saturates.

In Figure 20, the positive Y direction control current varies and the results of the analysis match the FE Methods with close correlation. This happens when the control current is less than 3A and force is less than 150N. When the Control current is increased beyond 3A, the attractive force on positive X direction is reduced as shown in Figure 19.

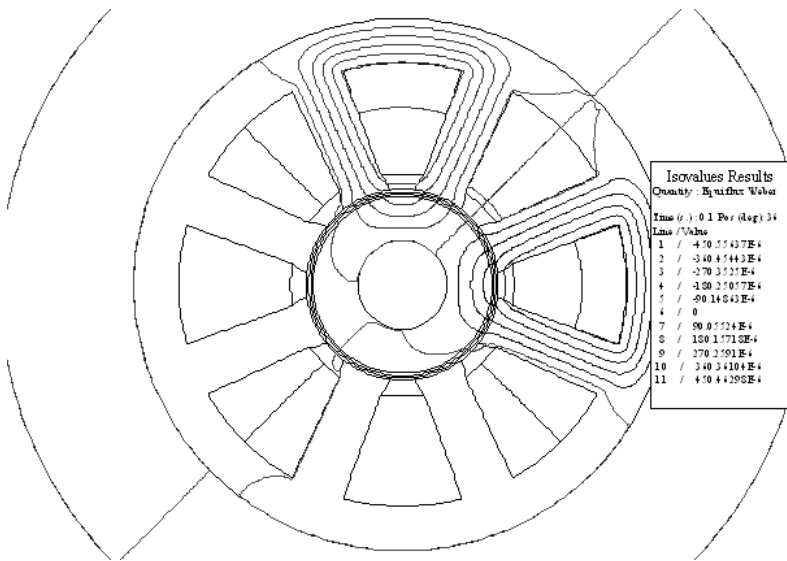


Figure 18: Flux in the radial magnetic bearing

This property is anticipated and contributes to the saturation of magnetic material on rotor; however, this is not important. The control current on the positive X direction is sinusoidal and on Y is co-sinusoidal for the Y direction in order to induce a rotating attractive force to offset the centrifugal force of flywheel. That means, when control current on the positive Y direction is more than 3A, the control current on the positive Y direction will be very small.

7. The present and future of the flywheel battery

The foregoing example has mainly focused on the electromagnetic analysis of the battery. The assumptions made with respect to the Halbach array would hold reasonably true. However, there are issues, for example, the requirement that battery self-discharge be less than 90% per month that may currently be viewed as an extreme demand. Consequently, a number of values obtained, like the rotor mass could be grossly at variance with reality. Moreover, the machine was assumed to behave ideally with respect to important issues, like rotor stresses, material properties and thermal dissipation.

The example, however, has importance, in that the off-grid household load depicted is unlike the most common terrestrial applications for flywheel batteries (like seamless power transfer during grid instability or short outages) whose purpose is mainly high power delivery for time bridging. Thus, the example provides a load magnitude and duration that are significantly different and helps to highlight issues that may not arise during the aforementioned common applications.

In general, current technical concerns for the flywheel battery technologists include structural

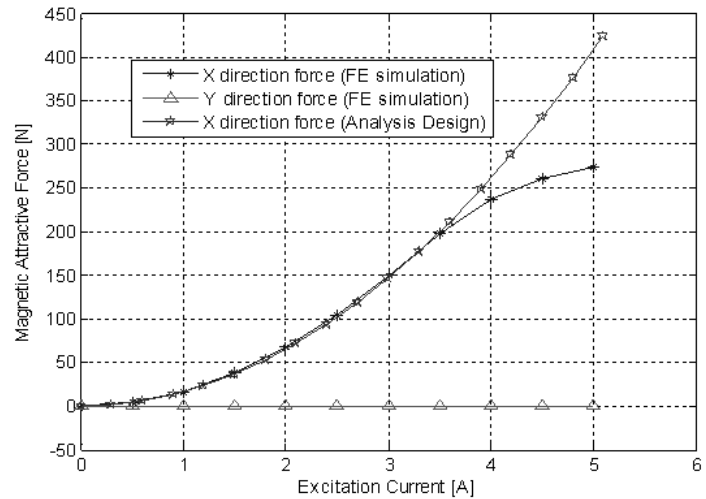


Figure 19: Attractive force versus positive X direction control current

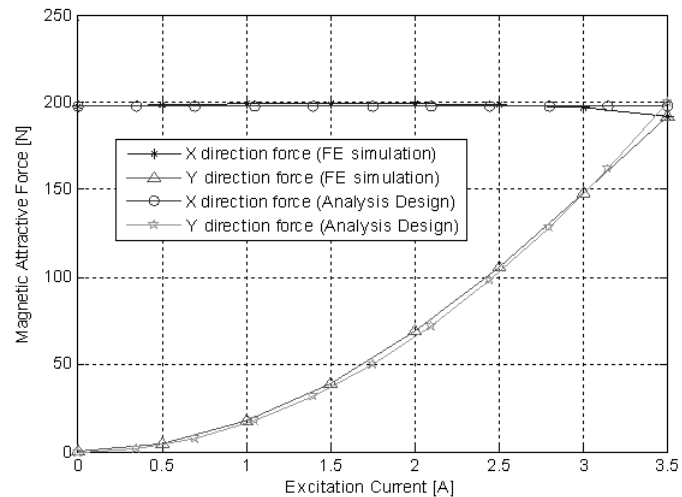


Figure 20: Attractive force versus positive Y direction control current

integrity of the rotor, the speed capability of the suspension bearings and the speed and power handling capability of the motor/generator and control electronics. Suspension bearings and motor/generator and drive technologies have applications in many other fields and have consequently seen relative advancement. Rotor structural integrity however, poses by far the biggest challenge in the development of the flywheel as a viable battery system. The issue is of such gravity and importance that the area of research transcends normal competition and groups of researchers have been developed to pool resources and assemble combined expertise (Pichot *et al.*, 1997).

Over the years, a variety of flywheel shapes from a range of materials have been designed with the aim to maximize the stored energy. The important parameters influencing failure of a rotor disk are fabrication imperfections (misfit), mean radius, thickness, material property, load gradation and speed. These are the sub-system indices of merit, all of which must be optimized simultaneously to achieve the best and most reliable design.

Numerous fibre materials exist including glass, graphite and carbon fibres. These have varying material strengths and are further differentiated by the reinforcements used during the construction process. The reinforcement (for example, epoxy) combines with the fibre to form a composite material. The epoxy or any other reinforcement with which it must be mixed has a substantially lower strength value, often of the order of 50%. The fibre constitutes only about 60% (by volume), resulting in a strength reduction of two. This then forms the design basis. Then one has to include allowances for fatigue. Fatigue is the systematic weakening of a material as a result of sustained stress over a period. This will vary depending on environmental factors like temperature and chemical corrosion due to water vapour.

The above considerations being for hoop strength alone, the designer will have to consider radial and axial strengths, which are also limited by the strength of the polymer matrix. For these forces, the fibre represents a discontinuity in the matrix and the design allowable should not exceed 15% of the matrix tensile strength. Structural stress issues do impact on the electrical design as well, for example, due to the fragility of the magnets forming the Halbach array, they must be assembled close to the hub. This compromises the power density of the generator. Along with rotor failures comes the problem of designing safe containment. As a consequence of these safety concerns, the PNGV later opted to defer development of the flywheel battery (as progress was deemed too slow to meet set deadlines of 2004 for concept model vehicles) but would continue to monitor progress in other programs mentioned later. In the case of a rural application,

however, underground containment has been found to satisfactorily address the safety concerns.

There is also great optimism as the carbon fibres strengths are projected to improve from the current strengths of 1 000 000 psi to 3 000 000 psi within this decade, implying a possible increase of 200% in stored kinetic energy. At this strength, the achievable material tip speeds will exceed 2 kilometres per second. Composite carbon fibre disks have an added safety advantage at failure. Unlike metallic disks, which disintegrate into dangerous solid shrapnel, in the case of a burst (which is the worst case scenario in rotor failure), fibre absorbs much of the energy by converting to cotton-like shred.

Another important factor is the cost. According to (Joseph *et al.*, 2002) the current cost of lead-acid batteries ranges between \$50–\$100 per kWh compared to \$400–\$800 per kWh for flywheel systems. This disparity currently gives the chemical batteries an edge. As for efficiency, flywheels (at 80 - 85%) are currently equal or better than state-of-the-art chemical batteries. Operational results of 93% have been reportedly achieved (Bitterly, 1998) by NASA and 90-95% (Chen *et al.*, 2009, Ribeiro *et al.*, 2001).

Lifespan is another major advantage of the flywheel battery, with estimates of at least 20 years as compared to between 3 and 5 years for chemical batteries. This is, however, compromised by their (currently) much higher self-discharge rates as compared to chemical batteries.

The biggest advantage held by flywheels, however, is that being an emerging technology, their potential has barely been tapped as compared to the centuries-old chemical systems which in all probability are unlikely to make major advances (Khartchenko, 1998). This is without considering environmental issues. At the forefront of rotor integrity and safety research is the Defense Advanced Research projects Agency (DARPA). In rotor dynamics, hub rim interface, strength optimisation and fatigue life are collaborations between independent groups with funding mainly from NASA. These include, Glen Research Centre (NASA GRC), Engineering Model Flywheel Energy Storage Systems, Small Business Research Contracts, Auburn Centre for Space Power and University of Texas/NASA Safe Life Criteria. Existing NASA and Boeing databases, like the Gas Turbine Engine Program are reinforcing efforts by University of Texas A&M, GRC and University of Virginia on high rpm developments, among others, that constitute the National Aerospace Flywheel Program.

8. Concluding remarks

The potential of the electromechanical battery has been highlighted as well as the shortcomings of continued use of chemical batteries. This paper has

examined the basics of kinetic energy storage as well as the machine design equations of an ironless permanent magnet synchronous motor-generator. Using these design equations a special battery supply for a rural African application has been specified. Pending research issues have been highlighted as well as the optimistic projections of the near future. With improved technologies it should therefore be possible, using machine design equations and given load requirements and availability of energy resources, to design an appropriate flywheel storage battery, that can be manufactured in Africa.

Moreover, the life cost cycle of the flywheel battery, which includes the potential for a long lifespan with virtually no maintenance as well as the positive environmental attributes are major advantages.

References

Arnold S. M., Saleeb A. F. and Al-Zoubi N. R. (2001). Deformation and Life analysis of composite flywheel disc and multi-disk systems. *NASA/TM-210578*.

Baaklini G. Y., Konno K. E. et al., (2001). NDE methodologies for composite flywheel certification. *SAE (01)3655*.

Bitterly J. G. (1998). Flywheel Technology: Past, Present and 21st Century projections. *IEEE AES Systems Magazine*.

Brushless Amplifiers, Servo Drives and Amplifiers, Advanced Motion Controls, 3805, Calle, Tecate, Camarillo, CA 93012, USA. <http://www.a-m-c.com/download/engnotes.pdf>.

Buchmann I. (2001). Can the Lead Acid battery compete in modern times? *Cardex Electronics Inc.* http://www.batteriesdigest.com/ask_isidor.htm

Chen H., Cong Y., Yang W., Tan C., Li Y. and Ding Y. (2009). Progress in electrical energy storage System: a critical review, *Prog. Nat. Sci.* 19 (3): pp. 291–312.

Halbach K. (1980). Design of permanent multi-pole magnets with oriented rare earth cobalt material. *Nuclear Instruments and Methods* 169: p1-10.

Hayes R. J., Kajis J. P. et al. (1999). Design and testing of a flywheel battery for a transit bus. *SAE (01)1159*.

Hebner R., and Aanstoos T. (2000). Energy Storage for sustainable systems: A white paper on the benefits and challenges of kinetic energy storage,” Centre for Electromechanics, University of Texas at Austin. <http://www.ece.gatech.edu/research/UCEP/2000-nsf/Presentations/Hebner.pdf>

Herbst J. D., Manifold S. M. et al. Design fabrication and testing of a 10MJ composite flywheel energy storage rotors. *SAE 981282*. <http://space-power.grc.nasa.gov/ppo/projects/flywheel/>

Hunt G. L. (1998). The great battery search. *IEEE Spectrum, November 1998*.

Joseph B., Hebner R., and Walls A. (2002). Flywheel Batteries Come Around Again. *IEEE Spectrum*, pages 46-51.

Khartchenko, N. (1998). Advanced Energy Systems. Taylor and Francis.

Bowler M.E. Flywheel energy systems: current status and future prospects. *Trinity flywheel power, San Francisco California*.

Mukund R. Patel. (1999). Flywheel Energy storage for spacecraft Power Systems. *SAE (01) 2589*.

Ofori-Tenkorang J., and Lang J. H. (1995). A comparative analysis of torque production in Halbach and conventional surface-mounted permanent-magnet synchronous motors. *IAS '95: Conference record of the IEEE Industry Applications conference*.

Pichot M. A., et al. (1997). Flywheel Battery Containment Problem. *Society of Automotive Engineers-970242*.

Post R. F. (1996). A new look at an old idea, the electro-mechanical battery. *Science and Technology Review* 1996.

Post R. F., Fowler T. K., and Post S. F. (1993). A High Efficiency Electromechanical Battery. *Proceedings of the IEEE*, (3) 81.

Review of the research program of the Partnership for a New Generation of Vehicles: Fifth Report (1999).(<http://www.nap.edu/open-book/0909064430/html/38.html>)

Ribeiro P. Johnson B., Crow M., Arsoy A and Liu Y. (2001). Energy storage systems for advanced power applications, *Proc. IEEE* 89 (12): pp. 1744–1756 .

Sebitosi A. B. and Pillay P. (2003). Applications of Advances in Automotive Electronics to Rural Electrification: The 42V Power-net for Rural Electrification. *Proceedings of the IEEE PES General Meeting 13*.

Seireg A. and Surana K. S. (1970). Optimum design rotating disk. *J. Engr. For industry, Trans. of the ASME*, 92: pp1-10.

Sung K. Ha, Dong-Gun Lee and-Jin Kim. Optimization of hybrid composite rotor in flywheel battery. *SAE 981899*.

Tsai S. W. and Wu E. M. (1971). A general theory of strength for anisotropic materials, *Journal of Composite Materials*.

Tsung-Ying Lee, Nanming Chen. (1993). Optimal capacity of the battery energy storage system in a power system. *IEEE Transactions on Energy conversion*, 8.

Received 11 October 2011; revised 4 June 2012